Hindawi
Mathematical Problems in Engineering
Volume 2022, Article ID 8024753, 21 pages
https://doi.org/10.1155/2022/8024753

Research Article

A Denoising Method for Ship-Radiated Noise Based on Optimized Variational Mode Decomposition with Snake Optimization and Dual-Threshold Criteria of Correlation Coefficient

Yuxing Li,[1,2] **Luqi Xiao**,[1] **Bingzhao Tang**,[1] **Lili Liang**,[1,2] **Yilan Lou**,[1] **Xinyao Guo**,[1] **and Xiaohui Xue**[1]

[1]*School of Automation and Information Engineering, Xi'an University of Technology, Xi'an 710048, China*
[2]*Shaanxi Key Laboratory of Complex System Control and Intelligent Information Processing, Xi'an University of Technology, Xi'an 710048, China*

Correspondence should be addressed to Yuxing Li; liyuxing@xaut.edu.cn

Received 23 May 2022; Revised 11 June 2022; Accepted 14 June 2022; Published 4 August 2022

Academic Editor: Baiyuan Ding

The ship-radiated noise (SN) is easily affected by other hydroacoustic objects or complex ocean noise when it spreads through water. In order to reduce the impact from the environment, a denoising method for SN based on optimized variational mode decomposition with snake optimization (SO-VMD) and dual-threshold criteria of correlation coefficient (CC) is proposed in this paper. The first step is to optimize the parameter combination, that is, decomposition number K and penalty factor α, of variational mode decomposition (VMD) by snake optimization (SO) with envelope entropy (EE). Then, the input signal using the optimized results is decomposed and the intrinsic mode functions (IMFs) are obtained. After that, the IMFs are classified into three classes with the dual-threshold criteria of CC, including signal components, signal-noise components, and noise components. Finally, all the signal components and the processed signal-noise components denoised by wavelet threshold (WT) are reconstructed together. Simulations performed in this paper demonstrate that SO is the more appropriate optimization for VMD and the proposed method has the more outstanding performance in denoising different kinds of test signals. In addition, experiments on measured SNs show that the proposed method is effective and accurate in denoising.

1. Introduction

Hydroacoustics is one of the hottest topics in marine science, and it is widely applied to many crucial fields. The ship-radiated noise (SN) is definitely one of the most vital research objects in hydroacoustics since it plays such a significant role in detection and defense [1–4]. However, complex ocean environment brings a mass of noise into SN which prevents it from detection, diagnosis, and so on. Thus, it is of paramount importance to denoise the SN effectively and accurately so that it could be processed more efficiently in the next step.

The traditional denoising methods are mainly based on Fourier transform, but unfortunately, it is unsuitable for many kinds of nonlinear and nonstationary signals. Therefore, WT is created with better time-frequency window characteristics. But the wavelet basis function and the number of decomposition layers greatly affect the effectiveness of denoising. To overcome the limitation, Huang et al. proposed a new adaptive decomposition algorithm named empirical mode decomposition (EMD) which can be used in processing nonlinear and nonstationary signals [5, 6]. The new idea aroused heated discussion in signal processing [7–9] but also had boundedness. Mode mixing and the end effect, which are two inevitable obstacles, severely influenced the effect of EMD denoising. In that case, many scholars dedicated themselves to conquering those two barriers. As a result, the progressive algorithms sprung up like mushrooms. Some popular algorithms, such as ensemble empirical mode decomposition (EEMD) [10, 11],

complete ensemble empirical mode decomposition (CEEMD) [12], complete ensemble empirical mode decomposition with adaptive noise (CEEMDAN) [13], and so on, are widely used in signal processing including denoising [14–16]. Unfortunately, none of them solved mode mixing and the end effect radically.

Dragomiretskiy and Zosso presented variational mode decomposition (VMD) which matches central frequency and bandwidth of each IMF adaptively [17]. The input signal is successfully decomposed into a series of IMFs recursively according to a precise mathematical model which is the reason why it can avoid mode mixing and the end effect. As the old saying goes, every coin has two sides. The decomposition effect of VMD highly depends on the decomposition number K and penalty factor α, named as parameter combination. At first, scholars focused on K, while being unaware of the influence of penalty factor α or the interaction between them. Scholars were gradually aware of the importance of penalty factor α, and then, optimization algorithms started to be introduced to search both two parameters. Tang et al. presented VMD optimized by particle swarm optimization (PSO) and constructed the fitness function of envelope entropy (EE) at the same time, which is used in rolling bearing fault diagnosis [18]. Yin et al. employed genetic algorithm (GA) to optimize VMD and continued to use EE as fitness function, which was used in structural damage diagnosis [19]. Ding et al. proposed a classification criteria of correlation coefficient (CC) in dividing IMFs into three classes when a new denoising method of MEMS gyroscope was presented [20]. Li et al. introduced gray wolf optimization (GWO) with permutation entropy (PE) and denoised IMFs with wavelet threshold (WT), aiming at denoising speech signals [21]. Chen and Zhao proposed a feature extraction method of early fault signals of rolling bearing based on VMD optimized by whale optimization algorithm (WOA) and creatively combined CC with L-kurtosis as fitness function [22]. They are frequently used in many fields instead of SN denoising. At the same time, the achievements obtained by Li et al. laid the foundation of SN research [23–26].

Recently, Hashim and Hussien presented a brand-new metaheuristic algorithm inspired by the mating behavior of snakes [27]. It strikes a brilliant balance between global searching and local searching and has not been imported in VMD optimizing. Inspired by its success, snake optimization (SO) and dual-threshold criteria are introduced to solve the adaptive parameter selection of VMD and the adaptive classification of IMFs, and a denoising method for SN based on SO-VMD and dual-threshold criteria of CC is proposed.

The structure of this paper is constructed as follows. Section 2 exhibits the theoretical background briefly. Section 3 shows the simulations on optimization algorithms and denoising methods. Section 4 demonstrates the experiments and analysis on actually measured SN of four kinds. Finally, the conclusions are drawn in Section 5.

2. Background Theories

2.1. Variational Mode Decomposition. VMD is a kind of self-adapting and nonrecursive decomposition algorithm which uses Hilbert transform and Wiener filter to construct constrained variational model and iteratively solves it. It is able to effectively decompose the input signal into several IMFs that have their unique sparse features. However, the key points of VMD algorithm are how to construct constrained variational model and solve it.

2.1.1. The Construction of Constrained Variational Model. First, the original signal would be decomposed into different IMFs defined as $u_k(k = 1, 2, 3, \ldots, K)$. Then, the algorithm obtains the analytic signal shown as equation (1) with Hilbert transform.

$$\left(\delta(t) + \frac{j}{\pi t}\right) * u_k(t). \tag{1}$$

Second, the algorithm evaluates the central frequency of each IMF and combines both by putting the latter as the exponential term of the former simultaneously, so that the IMF could be modulated into relevant base band shown as

$$\left[\left(\delta(t) + \frac{j}{\pi t}\right) * u_k(t)\right] * e^{-j\omega_k t}. \tag{2}$$

Eventually, the algorithm estimates the bandwidth of each IMF through the square L2-norm of the gradient of the demodulated signal. All the IMFs are FM-AM signals, and sum of them equals the original signal. The constrained variational model is shown as

$$\begin{cases} \min_{\{u_k\},\{\omega_k\}} \sum_{k=1}^{K} \left\| \partial \left[\left(\delta(t) + \frac{j}{\pi t}\right) * u_k(t) \right] e^{-j\omega_k t} \right\|_2^2, \\ \sum_{k=1}^{K} u_k = f, \end{cases} \tag{3}$$

where the value of K is the expected number of IMFs, f is the original input signal, $\omega_k(k = 1, 2, \ldots, K)$ is the central frequency of each IMF, $\delta(t)$ represents Dirac distribution, and $*$ represents the convolution operation.

2.1.2. The Solving Method of Constrained Variational Model. The key to solve constrained variational model is to transform it to unconstrained variational model. In that case, a quadratic penalty term α and Lagrangian multipliers $\lambda(t)$ are imported into the model to render it unconstrained. The expanded Lagrangian formula is as follows:

$$L(\{u_k\}, \{\omega_k\}, \lambda) = \alpha \sum_{k=1}^{K} \left\| \partial t \left[\left(\delta(t) + \frac{j}{\pi t}\right) * u_k(t) \right] e^{-j\omega_k t} \right\|_2^2 + \left\| f(t) - \sum_{k=1}^{K} u_k(t) \right\|_2^2 + \lambda(t), f(t) - \sum_{k=1}^{K} u_k(t), \tag{4}$$

where $\langle\cdot\rangle$ represents inner product operation.

By updating u_k, ω_k, and Lagrangian multipliers $\lambda(t)$ in the model, the algorithm uses a kind of iterative suboptimization called alternate direction method of multipliers (ADMM) to get the saddle point of the expanded Lagrangian formula, which is the solution to the original minimization problem. The updated method is expressed as

$$\begin{cases} \widehat{u}_k^{n+1}(\omega) = \dfrac{\widehat{f}(\omega) - \sum_{i>k}\widehat{u}_i^n(\omega) - \sum_{i>k}\widehat{u}_i^n(\omega) + \widehat{\lambda}^n(\omega)/2}{1 + 2\alpha\left(\omega - \omega_k^n\right)^2}, \\ \omega_k^{n+1} = \dfrac{\int_0^\infty \omega\left|\widehat{u}_k^{n+1}\right|^2 d\omega}{\int_0^\infty \left|\widehat{u}_k^{n+1}\right|^2 d\omega}, \\ \widehat{\lambda}^{n+1}(\omega) = \widehat{\lambda}^n(\omega) + \tau\left[\widehat{f}(\omega) - \sum_k \widehat{u}_k^{n+1}(\omega)\right], \end{cases} \tag{5}$$

where $\widehat{\ }$ means Fourier transform, n means the number of iterations whose initial value is 0, and τ represents the parameter of noise tolerance. The iteration will keep computing until achieving

$$\sum_k \left\|\widehat{u}_k^{n+1} - \widehat{u}_k^n\right\|_2^2 / \left\|\widehat{u}_k^n\right\|_2^2 < t, \tag{6}$$

where $s(s>0)$ is the threshold of iteration stop condition. Eventually, the final IMFs are generated by VMD.

2.2. Snake Optimization. SO is a kind of metaheuristic algorithm inspired by the mating behavior of snakes, proposed by Hashim and Hussien- in 2022. It strikes an appropriate balance of searching solutions between global-searching space and local-searching space.

SO algorithm generates random population in uniform distribution first, and then under the influence of both temperature $Temp$ and food quantity Q, the population chooses to enter the exploration phase or the exploitation phase. The exploration phase will lay stress on searching new solutions in the far neighborhood areas while the exploitation phase transforms the crucial searching space into already existed promising area. High exploration and low exploitation matching principle are constantly used by SO algorithm in the first half of iterations, and once it entered the second stage, the weight of the exploitation would dramatically increase to lock in the target. The updating principles of Temp and Q are shown below.

$$\begin{cases} \text{Temp} = \exp\left(\dfrac{-t}{T}\right), \\ Q = c_1 * \exp\left(\dfrac{t-T}{T}\right), \end{cases} \tag{7}$$

where t represents current iteration number, while T means the maximum of iteration number. The constant $c_1 = 0.5$.

When $Q < 0.25$, the algorithm searches for food in the vast searching space randomly, updating the relative position of food simultaneously. Obviously, it is the exploration phase, and the searching formulas belonging to it are shown as equations (8) and (9).

$$\begin{cases} X_{i,m} = X_{\text{rand},m} \pm c_2 \times A_m \times \left(\left(X_{\max} - X_{\min}\right) \times \text{rand} + X_{\min}\right), \\ A_m = \exp\left(\dfrac{-f_{\text{rand},m}}{f_{i,m}}\right), \end{cases} \tag{8}$$

$$\begin{cases} X_{i,f} = X_{\text{rand},f} \pm c_2 \times A_f \times \left(\left(X_{\max} - X_{\min}\right) \times \text{rand} + X_{\min}\right), \\ A_f = \exp\left(\dfrac{-f_{\text{rand},f}}{f_{i,f}}\right), \end{cases} \tag{9}$$

where $X_{i,m}$ represents the position of male snakes, while $X_{i,f}$ represents the position of female snakes, and $X_{\text{rand},m}$ and $X_{\text{rand},f}$ are identified as the random position of male and female snakes. The abilities of foraging of male and female snakes are indicated as A_m and A_f, respectively. $c_2 = 0.05$, and $r \in [0,1]$ is a random number. $f_{\text{rand},m}$ and $f_{\text{rand},f}$ represent the fitness of $X_{\text{rand},m}$ and $X_{\text{rand},f}$, respectively.

When $Q \geq 0.25$, which is reckoned as the food quantity is sufficient, it is time for exploitation. In this phase, two modes will be chosen: meal mode and courtship mode, and in courtship mode, fighting and mating are two inevitable circumstances. It is meal time for snakes when Temp > 0.6, and the courtship happens when Temp ≤ 0.6. Updating principles are as follows:

(a) Meal mode: in this mode, snakes would move close to the food, and the positions are calculated from the following equation:

$$X_{i,j}(t+1) = X_{\text{food}} \pm c_3 \times \text{Temp} \times \text{rand} \times \left(X_{\text{food}} - X_{i,j}(t)\right), \tag{10}$$

where $X_{i,j}$ is the position of all the individuals including both male and female and X_{food} represents the best position obtained so far, $c_3 = 2$.

(b) Courtship mode (fighting circumstance): to get the chance of mating, snakes of both genders would fight, and the relative equations are as follows:

$$\begin{cases} X_{i,m}(t+1) = X_{i,m}(t) \pm c_3 \times F_m \times \left(\left(X_{\text{best},f} - X_{i,m}(t)\right) \times \text{rand}\right), \\ F_m = \exp\left(\dfrac{-f_{\text{best},f}}{f_i}\right), \end{cases}$$
$$\begin{cases} X_{i,f}(t+1) = X_{i,f}(t) \pm c_3 \times F_f \times \left(\left(X_{\text{best},m} - X_{i,f}(t)\right) \times \text{rand}\right), \\ F_f = \exp\left(-\dfrac{f_{\text{best,m}}}{f_i}\right), \end{cases} \tag{11}$$

where F_m is the fighting ability of male snakes and relatively F_f is that of female snakes, and the best position of female snakes is expressed as $X_{best,f}$, while the best position of male snakes is expressed as $X_{best,m}$.

(c) Courtship mode (mating circumstance):

$$\begin{cases} X_{i,m}(t+1) = X_{i,m}(t) \pm c_3 \times M_m \times \left(Q \times X_{i,f}(t) - X_{i,m}(t)\right) \times \text{rand}\right), \\ M_m = \exp\left(\dfrac{-f_{i,f}}{f_{i,m}}\right), \end{cases}$$
$$\begin{cases} X_{i,f}(t+1) = X_{i,f}(t) \pm c_3 \times M_f \times \left(Q \times X_{i,m}(t) - X_{i,f}(t)\right) \times \text{rand}\right), \\ M_f = \exp\left(\dfrac{-f_{i,m}}{f_{i,f}}\right), \end{cases} \tag{12}$$

where M_m represents the mating ability of the male and M_f means the mating ability of the female.

After the eggs are hatched, the new generation is born, and the worst male and female individuals are replaced by the new according to

$$\begin{cases} X_{\text{worst},m} = X_{\min} + \left(X_{\max} - X_{\min}\right) \times \text{rand}, \\ X_{\text{worst},f} = X_{\min} + \left(X_{\max} - X_{\min}\right) \times \text{rand}. \end{cases} \tag{13}$$

It should be noted that $X_{\text{worst},m}$ and $X_{\text{worst},f}$ represent the worst individual of the male and female, respectively.

2.3. VMD Optimized by SO. For VMD algorithm, the preset of decomposition number K and quadratic penalty factor α has a great influence on the final effectiveness of decomposition. The close bound between them cannot be ignored; therefore, the searching of optimization should be comprehensive and synchronous. Due to the impressive

structure of SO algorithm, it is able to search for the better parameter combination effectively.

Speaking of the goal of searching, i.e., the fitness function, as envelope entropy (EE) shown in equation (14) could indicate the sparse features of a signal, the optimization is available using it as fitness function to obtain a triumph in parameter combination (K and α) searching. In a way, the lower the EE is, the more accurate the decomposition is.

$$\begin{cases} P_{i,j} = \dfrac{a_i(j)}{\sum_{j=1}^{N} a_i(j)}, \\ \\ E_i = -\sum_{j=1}^{N} P_{i,j} \lg p_{i,j}, \end{cases} \tag{14}$$

where $a_i(j)$ is the envelope signal obtained from the signal IMF and $P_{i,j}$ is the normalized form of the signal $a_i(j)$. The flowchart of optimized VMD by SO is shown in Figure 1.

2.4. Dual-Threshold Classification Criteria. CC can reflect the correlation between two signals; the higher the CC is, the more relevant they are, and vice versa. So, in that case, the CC of signal component is higher than that of noise component, which is an excellent evaluating standard in IMF classification.

Initially, CC between each IMF and the original signal is able to obtained with equation (15), and they are normalized to [0, 1]; then,

$$co(k) = \frac{\sum_{i=1}^{N} u_k(i) f(i)}{\sqrt{\sum_{i=1}^{N} u_k^2(i) . \sum_{i=1}^{N} f^2(i)}}, \tag{15}$$

where $co(k)$ is the CC of k_{th} IMF and N is the sample number of signal.

In the proposed classification criteria, the high threshold and the low one are both adaptive and are set for classifying the IMFs. The reason why they could be adaptive is that they are calculated according to the maximum CC and the average CC, which would change when signal changes. The IMF is recognized as signal component when its CC is bigger than the high one, while it is recognized as noise component when its CC is smaller than the low one, or the IMF is reckoned as the signal-noise component when its CC is both under the high and over the low. The adaptive thresholds are calculated by

$$\begin{cases} \text{th}H = \dfrac{co_{\max}}{\left(5 \times \left(co_{\max} - co_{\text{avg}}\right)\right)}, \\ \\ \text{th}L = \dfrac{co_{\max}}{\left(7 \times \left(co_{\max} - co_{\text{avg}}\right)\right)}, \end{cases} \tag{16}$$

where th$H$ represents the high threshold and th$L$ represents the low threshold, $co_{\max}$ is the maximum of all CC, and co_{avg} is the average of them.

2.5. Wavelet Threshold Denoising. WT denoising is one of the most popular denoising methods in use currently. It decomposes the input signal according to the chosen wavelet basis function, so as to obtain the relative wavelet coefficient. Then, compare the wavelet coefficient of each component with wavelet coefficient of the original signal, and the one with lower wavelet coefficient would be filtered, while the one with higher wavelet coefficient could be retained, and finally reconstruct them and finish WT denoising.

The effectiveness of the wavelet threshold denoising has a close bound with the set of its threshold and threshold function as well. Equations (17) and (18) give two threshold functions in common use, which are named as hard threshold and soft threshold, respectively.

$$\widetilde{\omega}_{j,k} = \begin{cases} \omega_{j,k}, & \left|\omega_{j,k} \geq \lambda\right|, \\ 0, & \left|\omega_{j,k} < \lambda\right|, \end{cases} \tag{17}$$

$$\widetilde{\omega}_{j,k} = \begin{cases} \text{sgn}\left(\omega_{j,k}\right)\left(\left|\omega_{j,k}\right| - \lambda\right), & \left|\omega_{j,k} \geq \lambda\right|, \\ 0, & \left|\omega_{j,k} < \lambda\right|, \end{cases} \tag{18}$$

where $\widetilde{\omega}_{j,k}$ is the evaluated wavelet coefficient, $\omega_{j,k}$ is the actual wavelet coefficient after decomposition, and λ is the evaluated threshold using unbiased risk estimation.

2.6. Proposed Denoising Method. In accordance with the theory above, the details of the proposed denoising method are expressed below and the flowchart of the SO-VMD-WT denoising method is in Figure 2.

Step 1. Use SO algorithm and EE to optimize the parameter combination, that is, K and α, of VMD algorithm with an appropriate iteration number and a population quantity, so as to obtain the best solution.

Step 2. Decompose the signal based on the best parameter combination and generate IMFs differentiated by their sparse features.

Step 3. Calculate CC of each IMF and obtain both high and low thresholds using the maximum and the average of all CCs, and then all the IMFs would be classified into three classes: signal components, signal-noise components, and noise components.

Step 4. Denoise the signal-noise components with the wavelet soft threshold denoising method. The soft threshold is shown in equation (15).

Step 5. Save the signal components and throw the noise components away and then reconstruct all the signal components and processed signal-noise components together.

3. Simulation and Analysis

3.1. Comparative Test of Optimization Algorithms. Aimed at proving SO algorithm is a much effective optimization

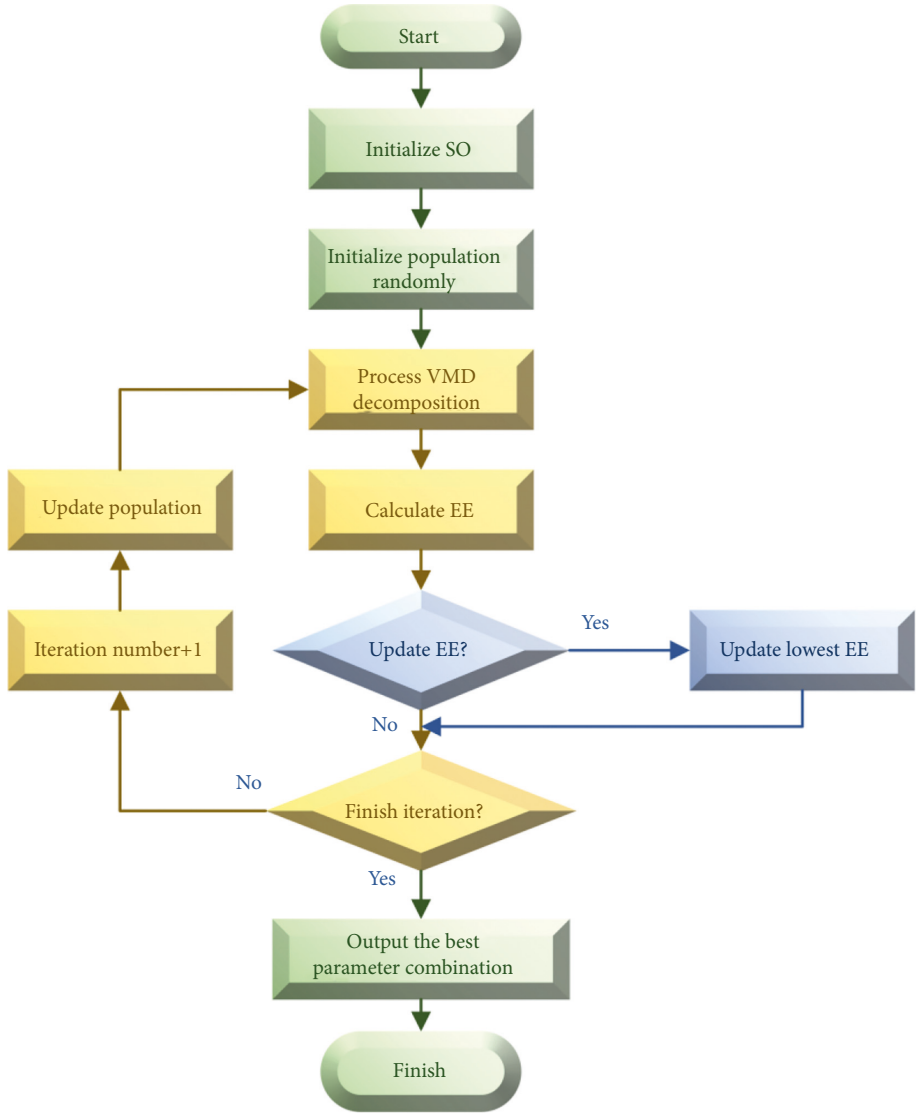

Figure 1: Flowchart of optimized VMD by SO.

algorithm than others in searching lowest EE of a signal after VMD, this section would give a statement of a comparative test of optimization algorithm in detail.

The test signal in use without noise is a combined signal shown as in Figure 3(a), which is composed of three different sinusoidal signals. Relatively, the noise signal whose SNR is 4 dB, named as TestSine (4 dB), is as shown in Figure 3(b), and their length $N = 1200$, and sample rate is 9500 Hz. The constituent parts are listed below:

$$\begin{cases} \text{TestSine} = v_1 + v_2 + v_3, \\ v_1 = 0.6 \sin(10\pi t), \\ v_2 = 0.4 \sin(50\pi t), \\ v_3 = 0.2 \sin(100\pi t). \end{cases} \tag{19}$$

Apparently, the signal has dramatically affected by noise and is hardly to diagnose. An immense number of glitches grow on the signal densely.

Three kinds of optimization algorithms are chosen for comparison, including GA, PSO, and WOA. Set iteration number as 50 and size of population as 10 equally in four algorithms. In GA algorithm, the parameter of crossing is set to 0.8, and the parameter of mutation is set to 0.1, while in PSO algorithm, the accelerated factors c_1 and c_2 are 1.5 likewise, the speed of K is limited between −1 and 1, and the speed of α is limited between −300 and 300. Also, the convergence curve of four algorithms in optimizing TestSine (4 dB), using EE as fitness function, is shown in Figure 4.

Figure 4 shows that SO is the best in searching lowest EE and WOA is at the second place, and PSO and GA are worse though. In order to avoid the affection of occasionality, 50 repeated experiments are carried out and the average results of different optimization algorithms are listed in Table 1.

An obvious conclusion could be drawn that PSO is fastest in four algorithms; however, SO is nearly as faster as PSO. On the other hand, SO does have the best searching

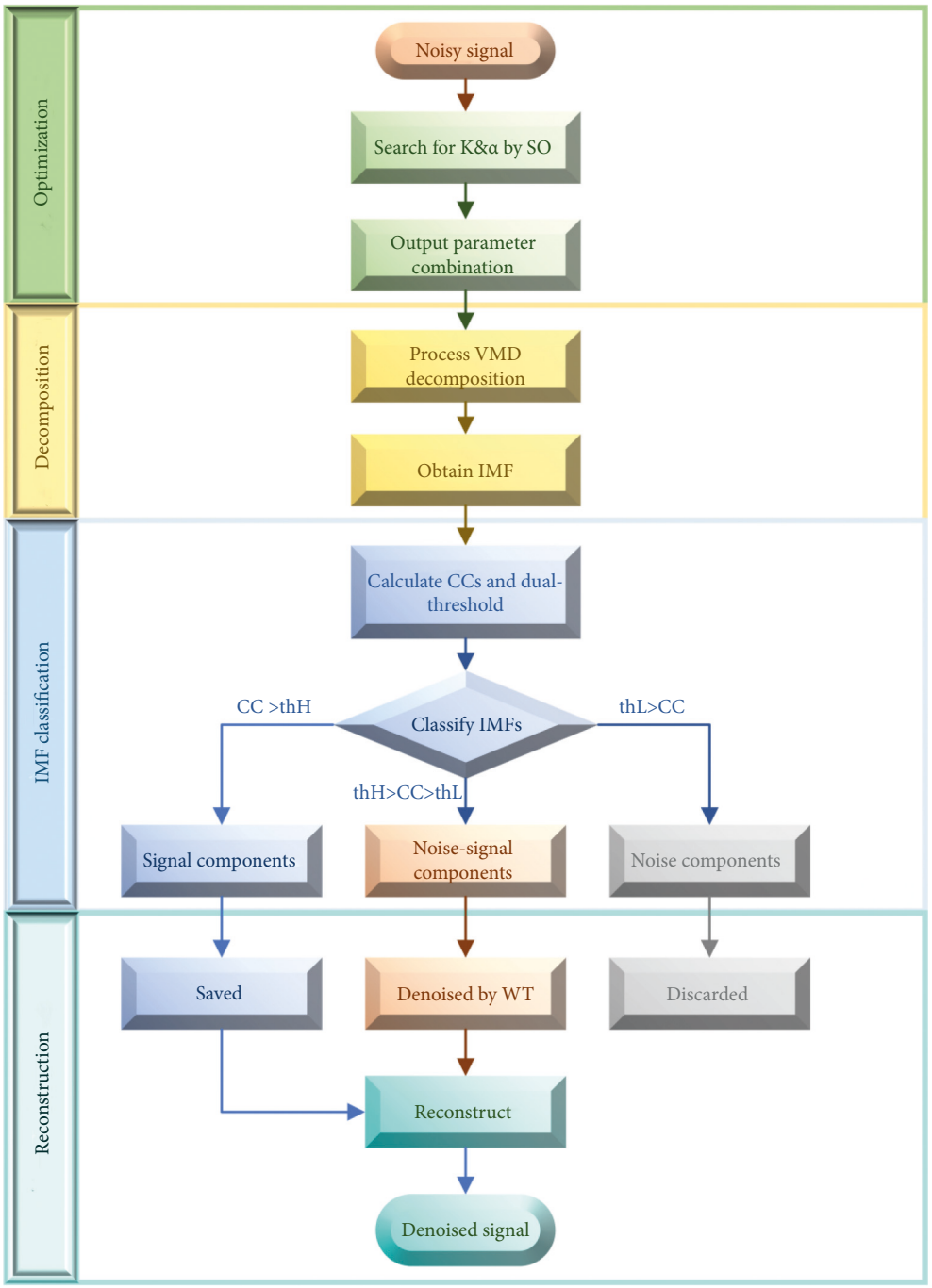

Figure 2: The flowchart of SO-VMD-WT denoising method.

ability, and GA and WOA are better than PSO. Therefore, SO should be used in VMD optimization theoretically and practically for its distinguished speed and precise searching.

3.2. Comparative Test of Denoising Methods. To investigate the denoising ability of the proposed method, the detailed simulation comparative experiments of different denoising methods are performed in this part.

3.2.1. Test Signals. Except for TestSine introduced in the previous section, four commonly used test signals shown in Figure 5 would be introduced as well. They are Blocks (Figure 5(a)), Bumps (Figure 5(c)), HeavySine (Figure 5(e)), and Doppler (Figure 5(g)), all generated by "wnoise" function in MATLAB with the length $N = 1024$. The relevant noisy signals with 4 dB SNR are also shown next. In the experiments, the five signals with six different noise situations are processed.

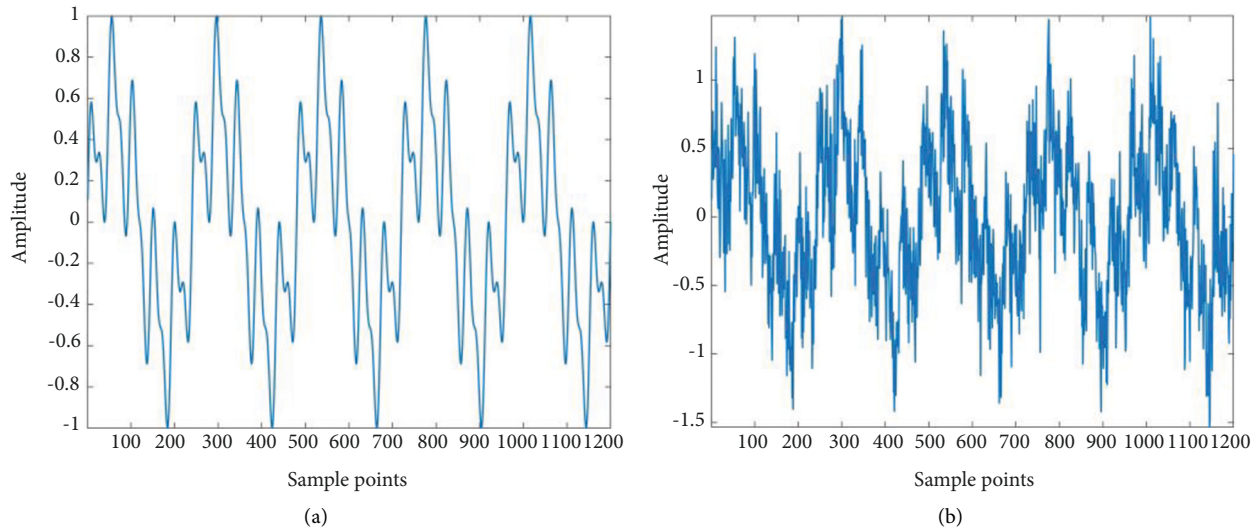

Figure 3: The waveforms of (a) TestSine and (b) TestSine (4 dB).

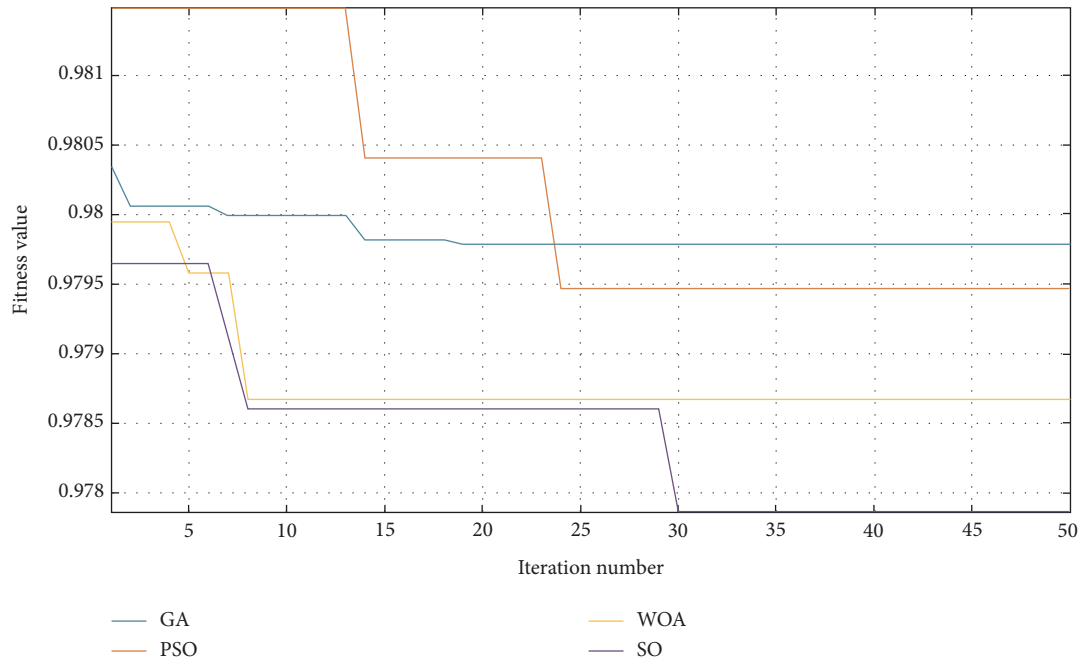

Figure 4: The convergence curve of four algorithms.

Table 1: The average results of different optimization algorithms.

Optimizations	GA	PSO	WOA	SO
The average iteration time	802.315	**690.211**	881.775	702.461
The average fitness result	0.978674	0.980568	0.978677	**0.978579**

3.2.2. Optimization and Decomposition. First, optimize the parameter combination by SO with ten snakes in a generation. After fifty iterations, the solution is obtained as $K = 10$, $\alpha = 1831$. The convergence curve of SO-VMD processing TestSine (4 dB) is shown in Figure 6.

Once the best parameter combination is obtained, the decomposition by VMD algorithm could be launched. The IMFs are all successfully acquired as shown in Figure 7. It is clear from the figure that different IMFs have different sparse features. Thus, the next step is to classify them accurately with effective classification criteria.

3.2.3. IMF Classification and Reconstruction. CC is able to reflect the similarity of signals, and the CC of signal component is much higher, while that of noise component is generally lower. Obviously, an essential step is to calculate the CC between each IMF and the input signal. The CC of IMF of TestSine (4 dB) is shown in Figure 8.

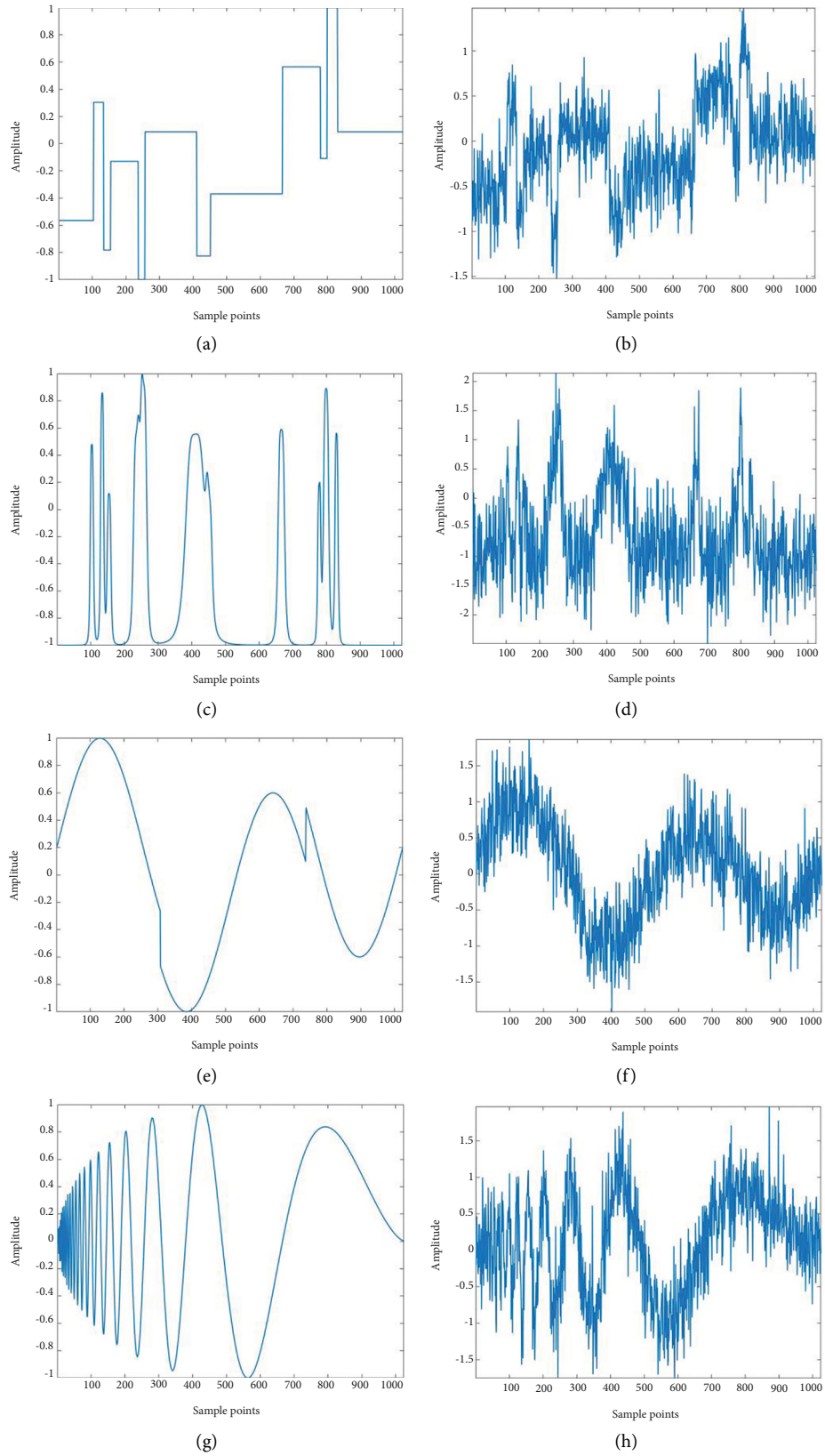

Figure 5: The waveform of four ordinary test signals. (a) Blocks. (b) Blocks (4 dB). (c) Bumps. (d) Bumps (4 dB). (e) HeavySine. (f) HeavySine (4 dB). (g) Doppler. (h) Doppler (4 dB).

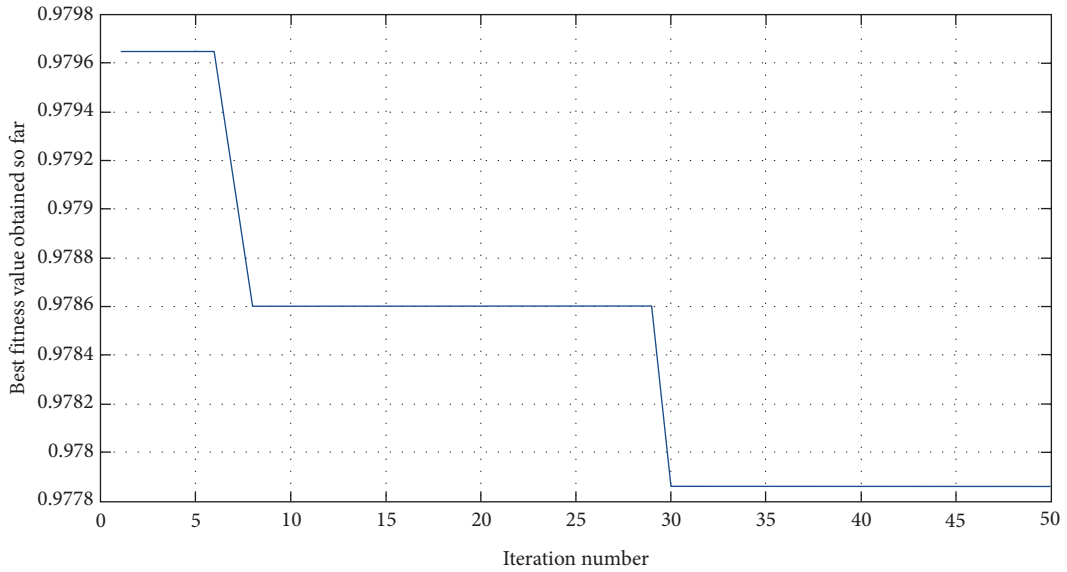

Figure 6: The convergence curve of SO-VMD processing TestSine (4 dB).

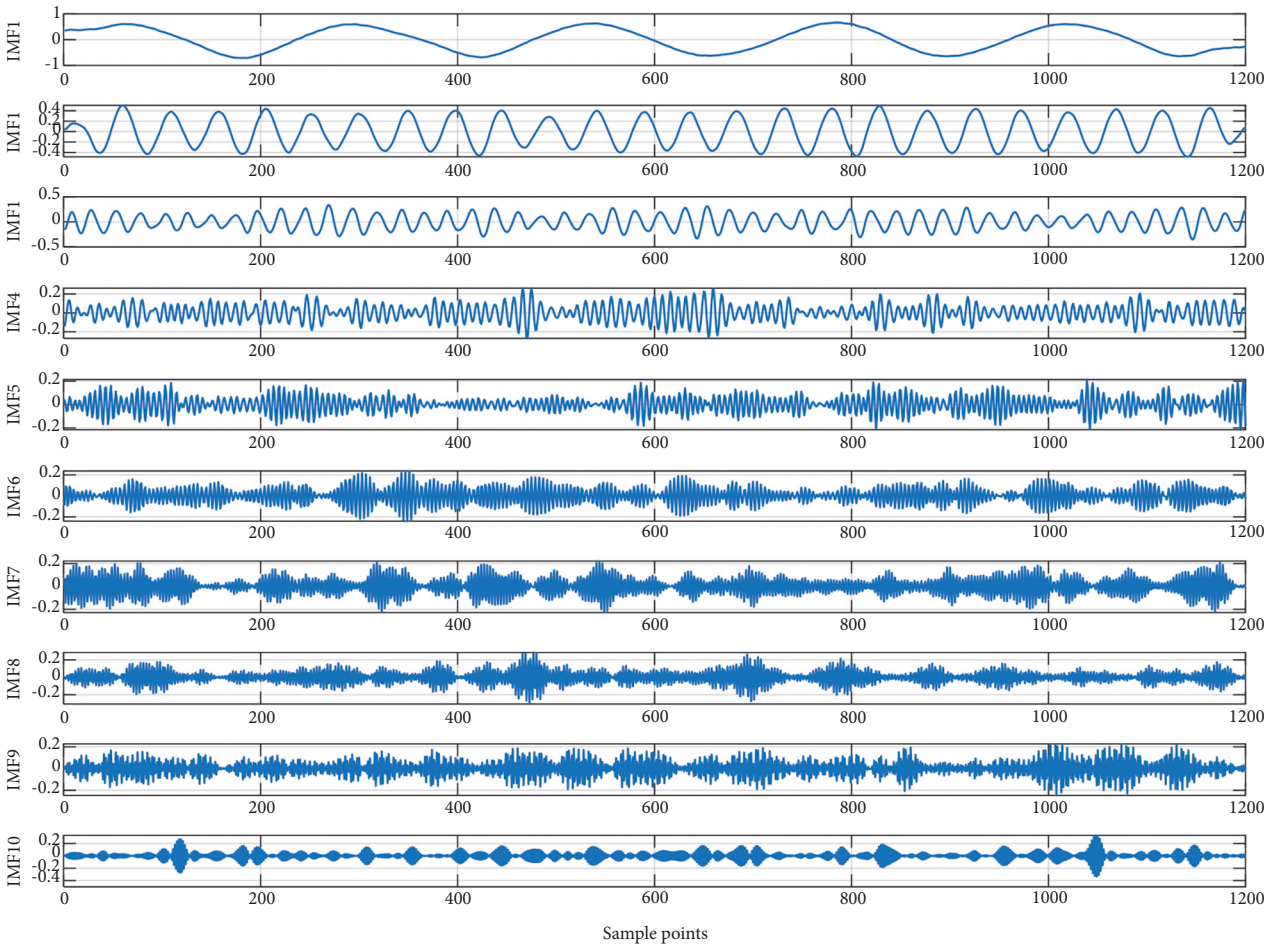

Figure 7: The IMFs of TestSine (4 dB) after SO-VMD.

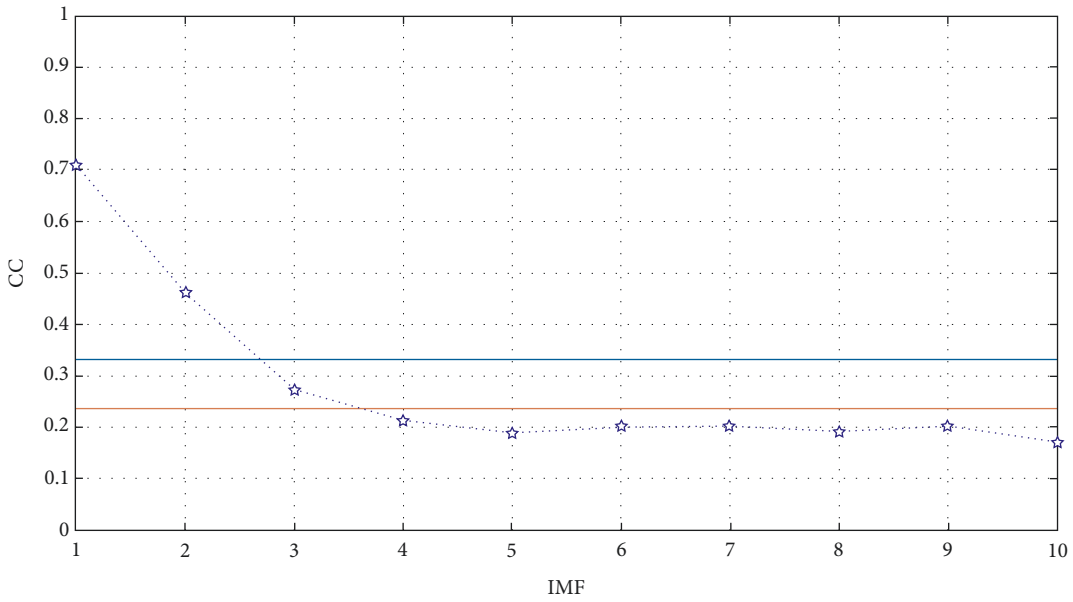

Figure 8: The CC of IMF of TestSine (4 dB).

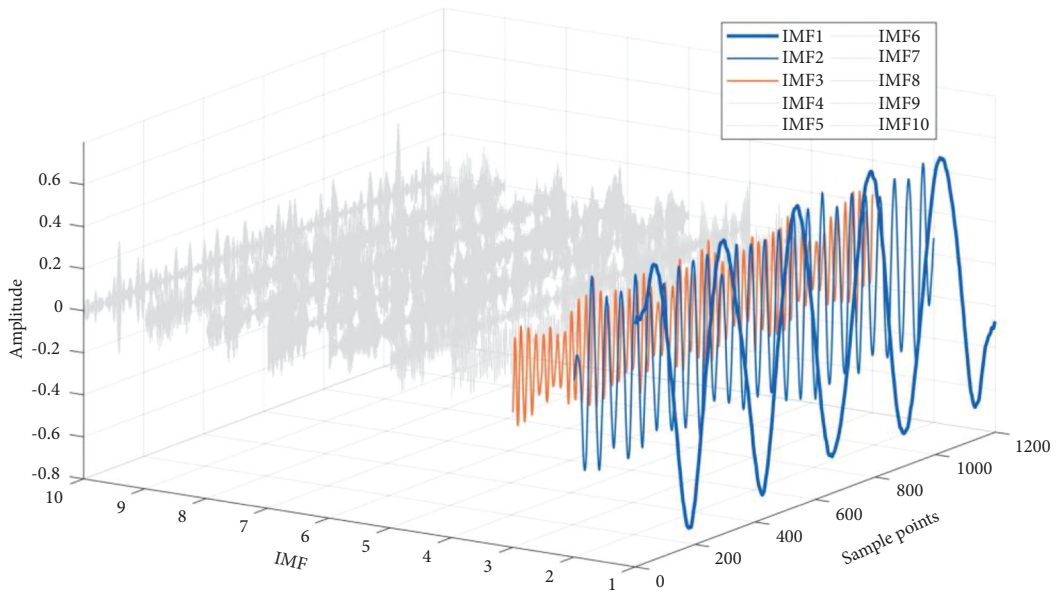

Figure 9: The classification result of IMF of TestSine (4 dB).

The blue horizontal line is the high threshold while the orange one is the low threshold. Obviously, the first two IMFs above the blue line are recognized as signal components, and the third IMF is strictly limited to the signal-noise class, and the rest of IMFs are all noise components whose CCs are nearly the same and below the orange line.

With the classification finishing, the denoising step is carried out. The classification result of TestSine (4 dB) IMF is shown in Figure 9.

As what is designed above and shown in Figure 9 as well, the signal components in blue would be saved, the signal-noise components in orange are supposed to be denoised by WT with soft threshold, and unfortunately, the noise components in gray are all given up for signal residuals barely existing in them.

At last, realize the final reconstruction of all the processed signal-noise components and signal components together. The denoising result of TestSine (4 dB) and the noiseless TestSine is shown in Figure 10.

Indeed, the effectiveness of the proposed method is impressive as the SNR increases from 4 dB to 14.274 dB, the RMSE drops down to 0.1023, and the CC between the denoising signal and the noiseless signal rises to 0.9828.

3.2.4. Comparative Analysis. In the comparative experiments, WT denoising, denoising based on EMD and

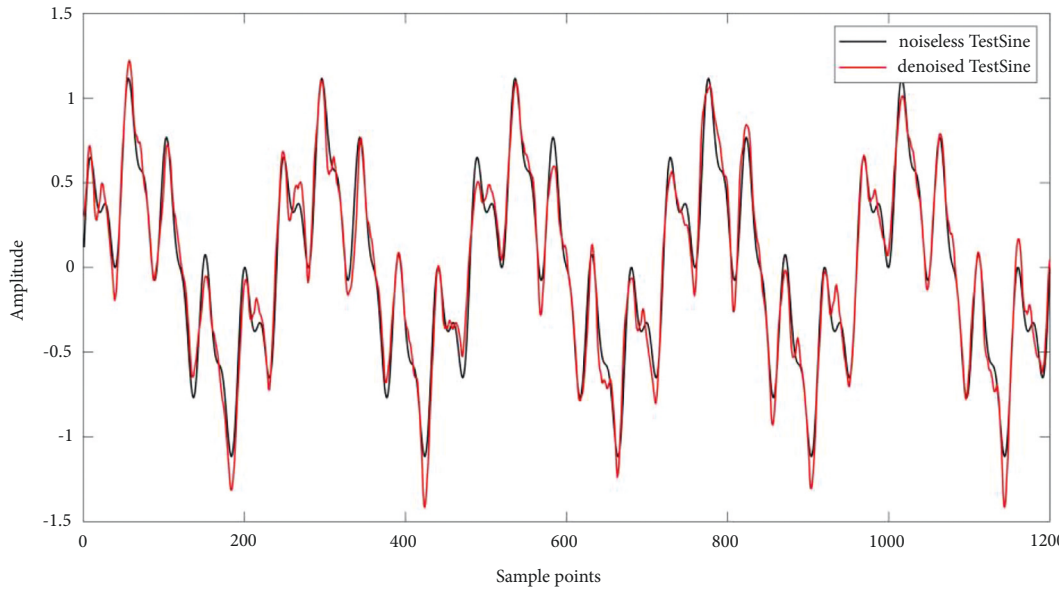

Figure 10: The denoising result of TestSine (4 dB).

Table 2: Denoising results of TestSine with four methods.

SNR (dB)	Parameters	Denoising methods				
		WT	EMD-WT	EEMD-WT	VMD-WT	Proposed
0	SNR	8.1976	8.7099	9.9988	9.5354	**10.3930**
	RMSE	0.2059	0.1941	0.1674	0.1765	**0.1599**
	CC	0.9229	0.9417	0.9494	0.9461	**0.9548**
2	SNR	10.2846	10.2967	11.2981	11.7406	**12.8612**
	RMSE	0.1619	0.1617	0.1441	0.1370	**0.1204**
	CC	0.9520	0.9534	0.9630	0.9662	**0.9740**
4	SNR	11.1976	12.2047	12.4446	13.1963	**14.2740**
	RMSE	0.1458	0.1298	0.1263	0.1158	**0.1023**
	CC	0.9615	0.9728	0.9711	0.9761	**0.9828**
6	SNR	14.8280	14.9080	14.7257	15.4013	**16.0250**
	RMSE	0.0960	0.0951	0.0971	0.0899	**0.0836**
	CC	0.9834	0.9841	0.9832	0.9856	**0.9880**
8	SNR	16.3035	16.8705	16.1931	16.1152	**18.1958**
	RMSE	0.0810	0.0759	0.0820	0.0828	**0.0651**
	CC	0.9883	0.9897	0.9879	0.9877	**0.9926**
10	SNR	17.1184	17.4387	17.5460	16.7752	**19.7818**
	RMSE	0.0737	0.0711	0.0702	0.0767	**0.0543**
	CC	0.9903	0.9910	0.9914	0.9897	**0.9949**

WT (EMD-WT), denoising based on EEMD and WT (EEMD-WT), and denoising based on VMD and WT (VMD-WT) are used as the compared objects. What should be noticed is that all the WT denoising processes use soft threshold, and in all methods, the IMFs are classified into three classes, the first refers to signal components, the second refers to signal-noise components which need to be denoised by WT, and the third refers to noise components which tend to be discarded. The proposed method is SO-VMD-WT. For VMD-WT, the only difference between itself and the proposed method is that the parameter combination is not optimized in advance but settled directly. The comparative results with different input signals are given in Tables 2–6, and each kind of averaged data is attained after five repeated tests.

For TestSine, different denoising methods improve its SNR in different levels, the proposed method rises it about 10 dB, and others rise it about 7 dB though. Similarly, RMSE decreases and CC increases the most with the proposed method than others. The same phenomenon appears in the other tests. Since other test signals are nonlinear, the results

Table 3: Denoising results of Blocks with four methods.

SNR (dB)	Parameters	Denoising methods				
		WT	EMD-WT	EEMD-WT	VMD-WT	Proposed
0	SNR	0.7476	8.3567	9.3907	9.4306	**10.4939**
	RMSE	2.7252	1.1348	1.0075	1.0029	**0.8873**
	CC	0.7482	0.9322	0.9498	0.9441	**0.9566**
2	SNR	3.2493	10.1978	11.4891	11.7487	**12.6145**
	RMSE	2.0432	0.9181	0.7913	0.7680	**0.6951**
	CC	0.8394	0.9570	0.9649	0.9665	**0.9735**
4	SNR	6.0447	11.3690	12.2761	12.2372	**13.7856**
	RMSE	1.4809	0.8023	0.7227	0.7260	**0.6074**
	CC	0.8936	0.9634	0.9700	0.9697	**0.9794**
6	SNR	9.5823	13.5367	13.5051	13.9071	**14.4972**
	RMSE	0.9855	0.6251	0.6274	0.5990	**0.5596**
	CC	0.9493	0.9783	0.9776	0.9795	**0.9825**
8	SNR	13.8537	14.1308	14.6395	14.7323	**15.3228**
	RMSE	0.6027	0.5838	0.5506	0.5447	**0.5089**
	CC	0.9795	0.9805	0.9829	0.9832	**0.9853**
10	SNR	15.9326	15.4508	15.6854	15.4337	**16.3864**
	RMSE	0.4744	0.5015	0.4881	0.5024	**0.4503**
	CC	0.9872	0.9859	0.9864	0.9856	**0.9885**

Table 4: Denoising results of Bumps with four methods.

SNR (dB)	Parameters	Denoising methods				
		WT	EMD-WT	EEMD-WT	VMD-WT	Proposed
0	SNR	1.7856	7.9196	7.9827	9.1552	**10.6169**
	RMSE	1.4652	0.7231	0.7179	0.6272	**0.5301**
	CC	0.7796	0.9246	0.9220	0.9391	**0.9557**
2	SNR	5.4042	9.3199	9.7503	10.9863	**12.1982**
	RMSE	0.9660	0.6154	0.5857	0.5080	**0.4418**
	CC	0.8737	0.9470	0.9460	0.9600	**0.9698**
4	SNR	10.6910	11.1315	11.3874	12.7153	**13.9820**
	RMSE	0.5256	0.4996	0.4851	0.4163	**0.3598**
	CC	0.9599	0.9613	0.9649	0.9730	**0.9798**
6	SNR	13.6885	13.7245	12.4491	14.5784	**15.3242**
	RMSE	0.3722	0.3706	0.4293	0.3359	**0.3083**
	CC	0.9786	0.9793	0.9715	0.9825	**0.9856**
8	SNR	15.2112	14.0420	14.5142	15.9091	**17.1153**
	RMSE	0.3123	0.3573	0.3384	0.2882	**0.2509**
	CC	0.9851	0.9802	0.9827	0.9874	**0.9902**
10	SNR	16.2731	14.3585	16.6770	16.6911	**18.2476**
	RMSE	0.2764	0.3446	0.2638	0.2634	**0.2202**
	CC	0.9885	0.9815	0.9892	0.9897	**0.9926**

of each methods change distinctly as well. Although signals in various frequencies especially in high frequency, take Doppler for example, are difficult to denoise, the proposed method performs the best of all methods since VMD is good at elaborate decomposing.

In the global view of comparative experiments, the performance of WT is worse than others to some degree, and EMD-WT is better than WT, and EEMD-WT mostly does better in denoising than WT and EMD-WT, while VMD-WT is the second place generally; the proposed method has the most brilliant performance in denoising than the other four denoising methods, whatever the input signal is or how much noise it has.

4. Experiments of SN and Analysis

4.1. Preparations

4.1.1. Four Kinds of SN. In the denoising experiments of actual measured signals, four kinds of SN are chosen with noise of different levels. Figure 11 lists all the waveforms of four classes of SN after they are normalized to [−1, 1] and sampled with length $N = 10000$ and frequency $f = 52734$ Hz. The four signals represent four unique kinds of ships which are under different circumstances.

It could be seen that such bad noises affect each signal because there are a number of glitches appearing on it.

Table 5: Denoising results of HeavySine with four methods.

SNR (dB)	Parameters	Denoising methods				
		WT	EMD-WT	EEMD-WT	VMD-WT	Proposed
0	SNR	0.8011	7.5619	12.1280	12.9952	**13.6321**
	RMSE	2.8139	1.2920	0.7638	0.6912	**0.6423**
	CC	0.7350	0.9193	0.9790	0.9758	**0.9811**
2	SNR	3.0895	11.0908	13.5031	15.4233	**16.1756**
	RMSE	2.1622	0.8607	0.6520	0.5226	**0.4793**
	CC	0.8272	0.9649	0.9782	0.9866	**0.9904**
4	SNR	5.8254	12.6017	15.5310	16.5060	**18.9723**
	RMSE	1.5780	0.7233	0.5162	0.4614	**0.3473**
	CC	0.8897	0.9729	0.9860	0.9889	**0.9942**
6	SNR	8.8552	14.3753	16.9747	19.5505	**20.4007**
	RMSE	1.1133	0.5897	0.4372	0.3250	**0.2947**
	CC	0.9386	0.9822	0.9899	0.9945	**0.9955**
8	SNR	13.8275	16.6044	18.1212	20.7650	**21.5420**
	RMSE	0.6281	0.4562	0.3831	0.2826	**0.2584**
	CC	0.9795	0.9895	0.9928	0.9958	**0.9967**
10	SNR	18.4623	18.8292	19.8101	22.1090	**23.8117**
	RMSE	0.3683	0.3531	0.3154	0.2421	**0.1990**
	CC	0.9930	0.9937	0.9948	0.9973	**0.9979**

Table 6: Denoising results of Doppler with four methods.

SNR (dB)	Parameters	Denoising methods				
		WT	EMD-WT	EEMD-WT	VMD-WT	Proposed
0	SNR	8.4732	8.4764	8.7907	10.4188	**11.1990**
	RMSE	0.1104	0.1104	0.1065	0.0883	**0.0807**
	CC	0.9370	0.9336	0.9369	0.9547	**0.9613**
2	SNR	10.2841	10.2706	10.9017	11.0601	**12.2664**
	RMSE	0.0896	0.0898	0.0835	0.0820	**0.0713**
	CC	0.9592	0.9564	0.9598	0.9600	**0.9702**
4	SNR	11.8894	11.3546	11.3254	11.9327	**12.9705**
	RMSE	0.0745	0.0792	0.0795	0.0741	**0.0658**
	CC	0.9679	0.9639	0.9639	0.9674	**0.9745**
6	SNR	13.4078	12.5488	12.5963	13.1249	**14.1368**
	RMSE	0.0626	0.0691	0.0687	0.0646	**0.0575**
	CC	0.9777	0.9719	0.9721	0.9754	**0.9805**
8	SNR	14.2086	13.8491	13.5727	14.2939	**15.3702**
	RMSE	0.0570	0.0595	0.0614	0.0565	**0.0499**
	CC	0.9810	0.9794	0.9781	0.9813	**0.9854**
10	SNR	15.4667	13.9908	13.9214	15.6713	**16.4196**
	RMSE	0.0494	0.0585	0.0590	0.0482	**0.0442**
	CC	0.9858	0.9799	0.9796	0.9864	**0.9887**

Apparently, dramatic impulses happen accidentally owing to the equipment fault or some other reasons.

4.1.2. Evaluation Criterion. In case of no noiseless signal to be compared, a brand-new evaluation criterion which relies on the attractor trajectories is proposed. Attractor trajectory is a well-known description in chaos theory. It is greatly sensitive to the initial conditions because it exhibits totally distinct shapes with any tiny changes of initial conditions. Speaking of the signal, noiseless signal tends to have a smooth and regular trajectory while noisy signal possesses a disordered and irregular trajectory. Thus, the effectiveness of denoising can be shown as the changing of attractor trajectories.

4.2. Denoising Experiments

4.2.1. Optimization and Decomposition. Take SN-iii for example, a 10000-sample-points-long signal is inputted first. Then, optimize the parameter combination of VMD by SO with the initial conditions preset as 10 for popular number and 300 for iteration number. The iteration chart of SN-iii is exhibited in Figure 12.

The results of optimization after iterative searching are $K = 8$ and $\alpha = 68473$. With the solution of optimization, the

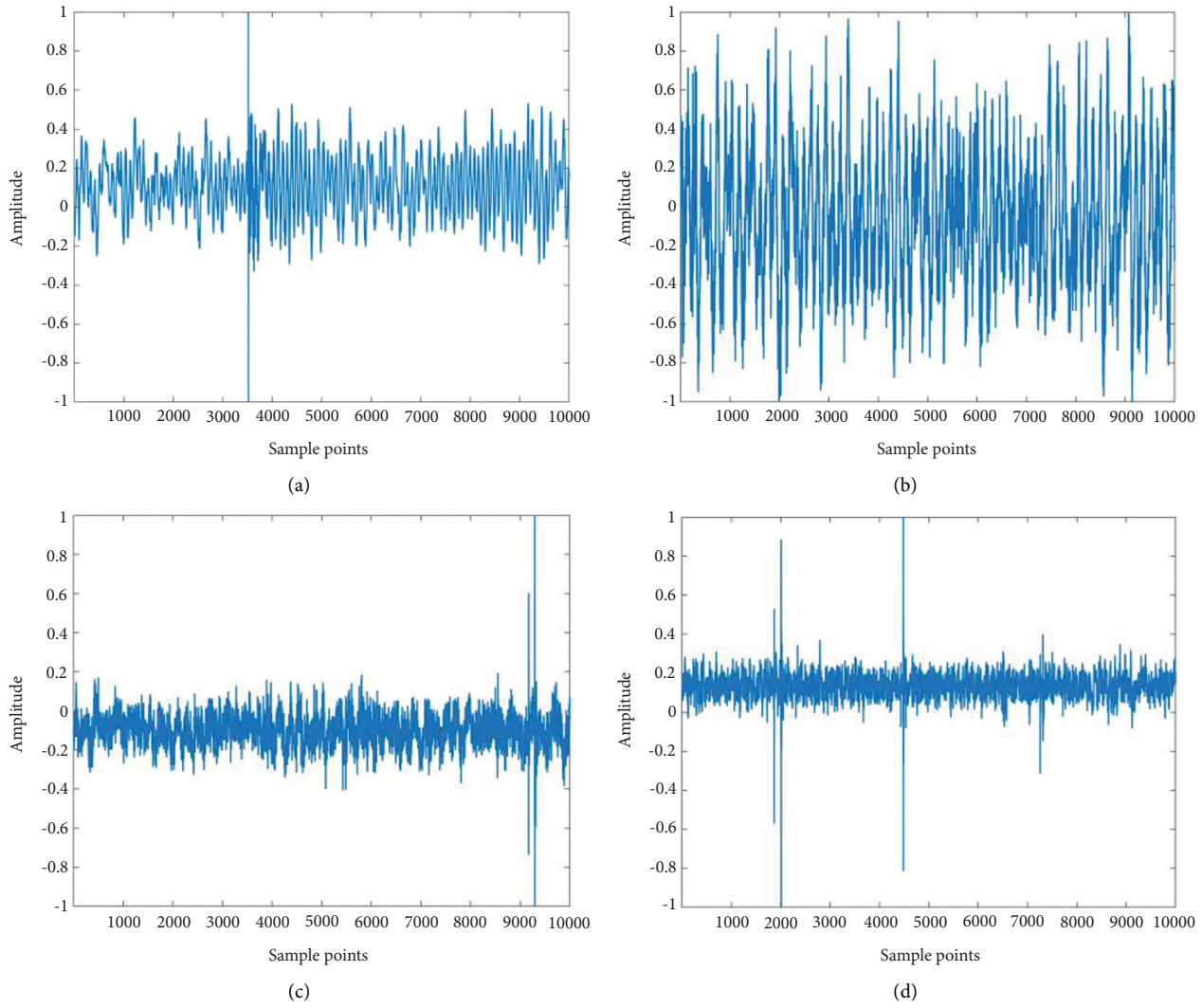

Figure 11: The waveform of four classes of SN. (a) SN-i. (b) SN-ii. (c) SN-iii. (d) SN-iv.

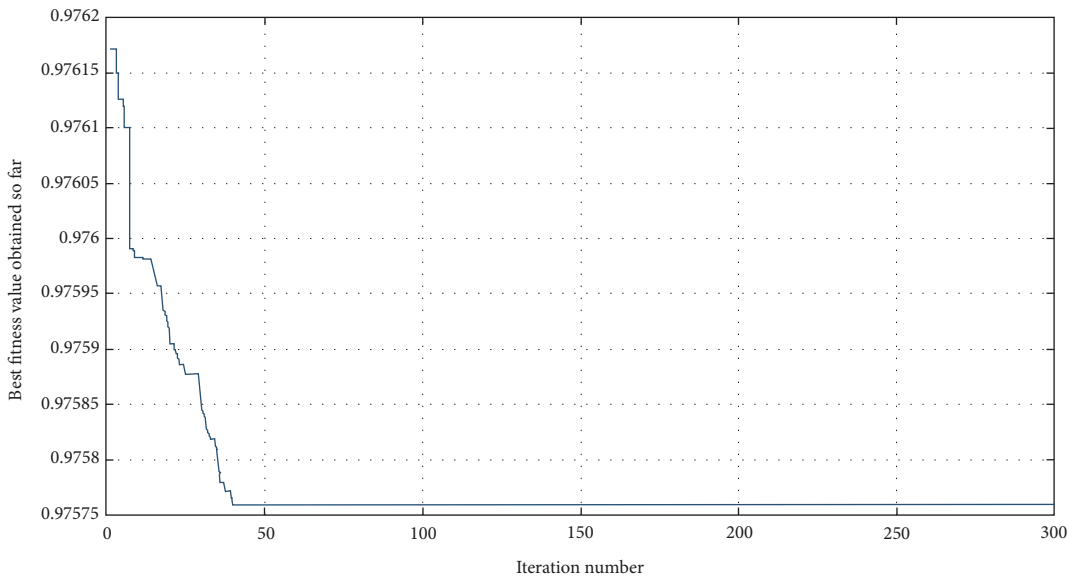

Figure 12: The iteration chart of SN-iii.

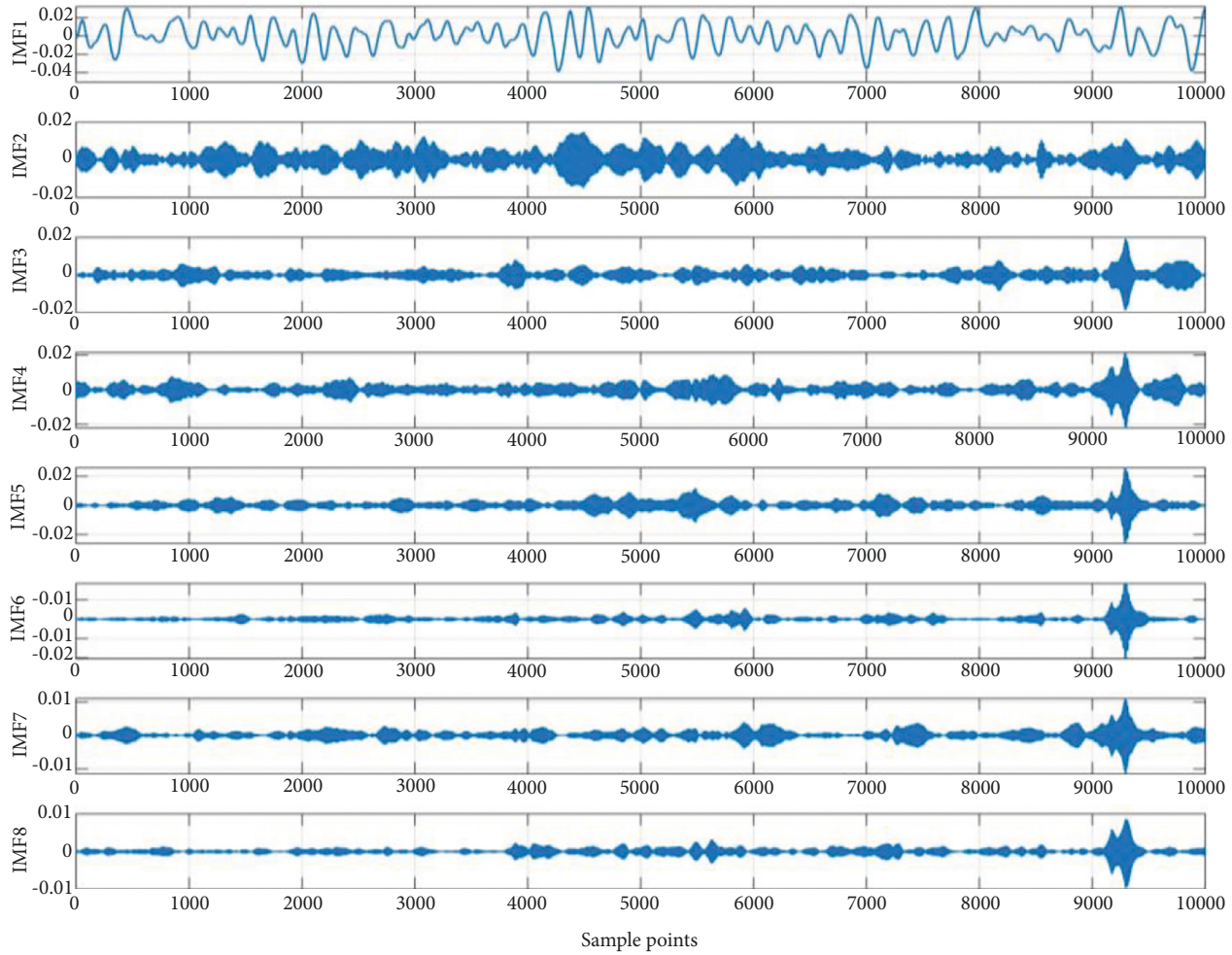

Figure 13: The IMFs of SN-iii.

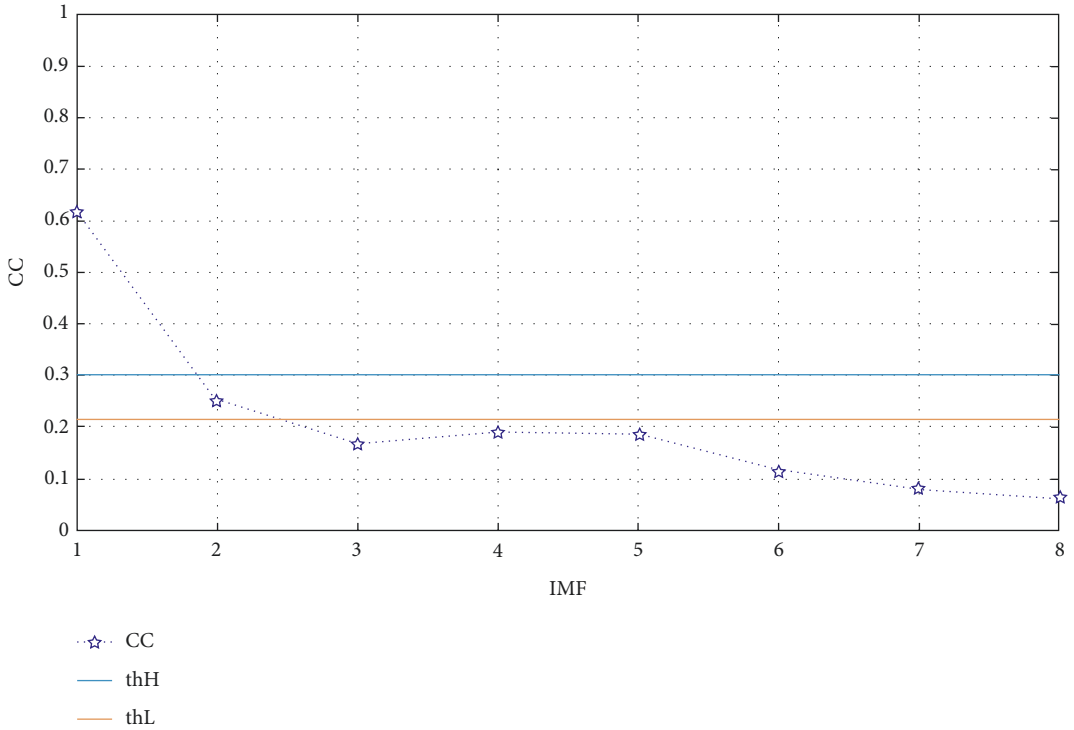

Figure 14: The CC of IMF of SN-iii.

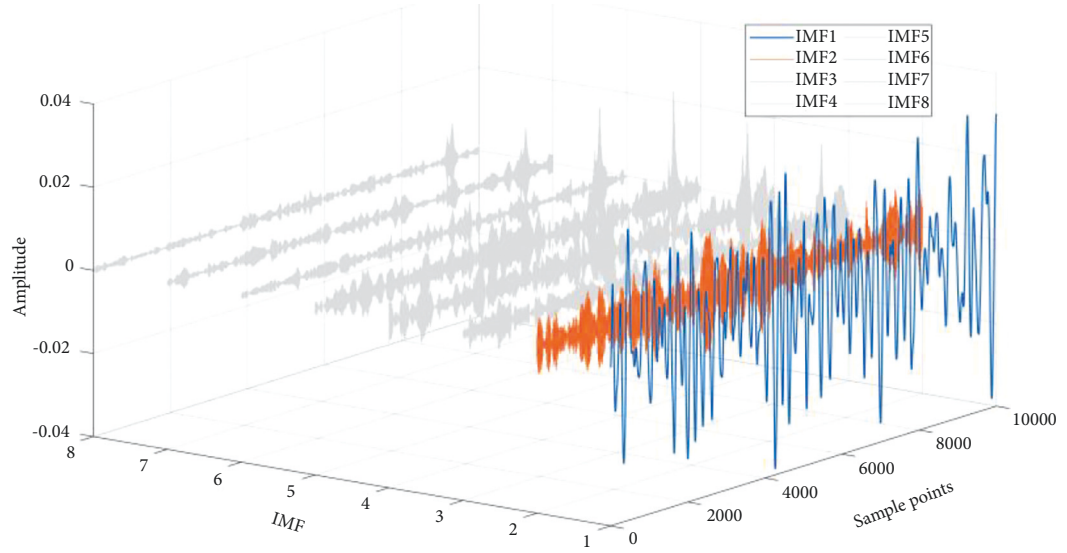

Figure 15: The classification result of SN-iii.

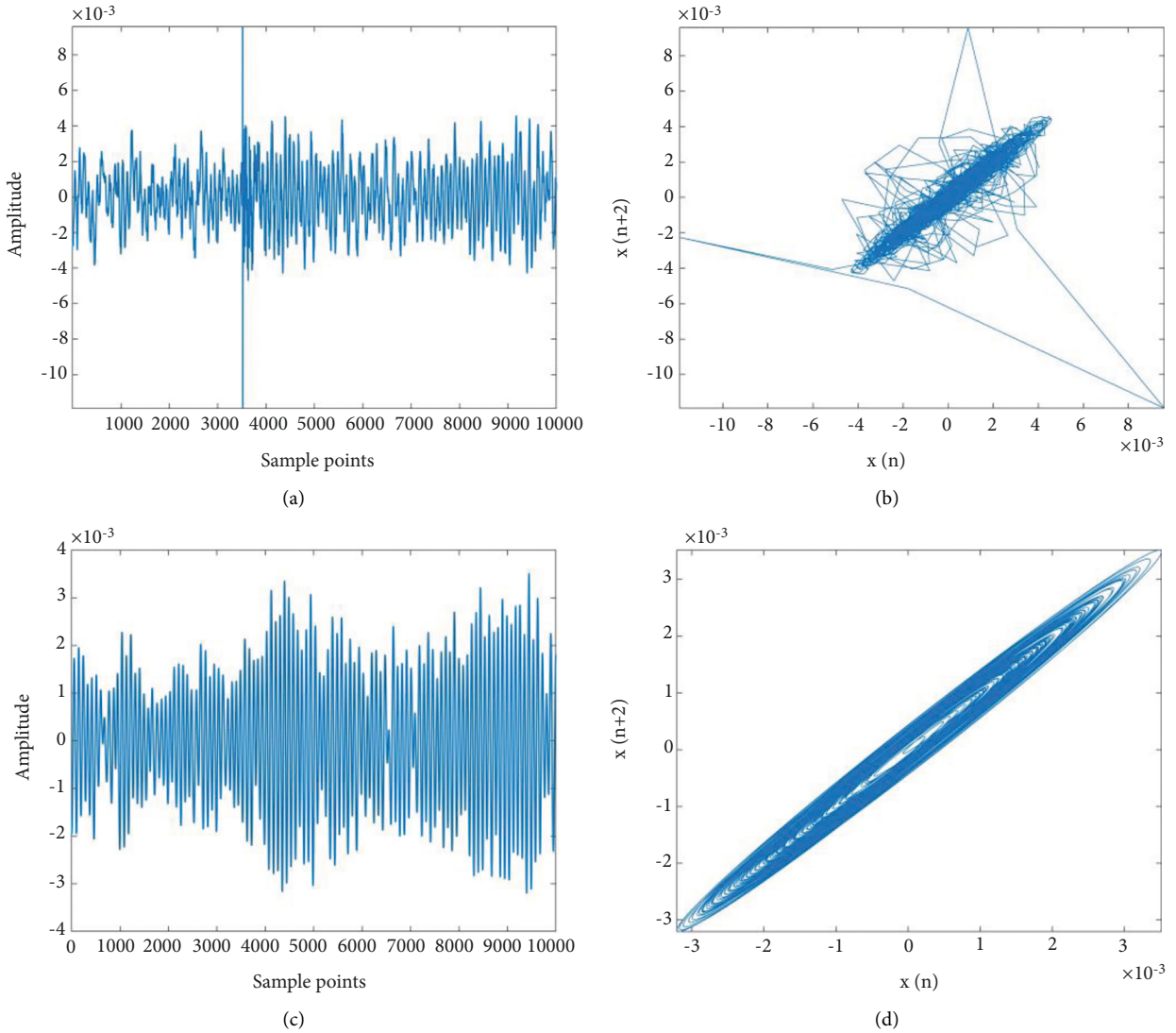

Figure 16: The waveforms and attractor trajectories of original and denoised SN-i. (a) The waveform of SN-i. (b) The attractor trajectories of SN-i. (c) The waveform of denoised SN-i. (d) The attractor trajectories of denoised SN-i.

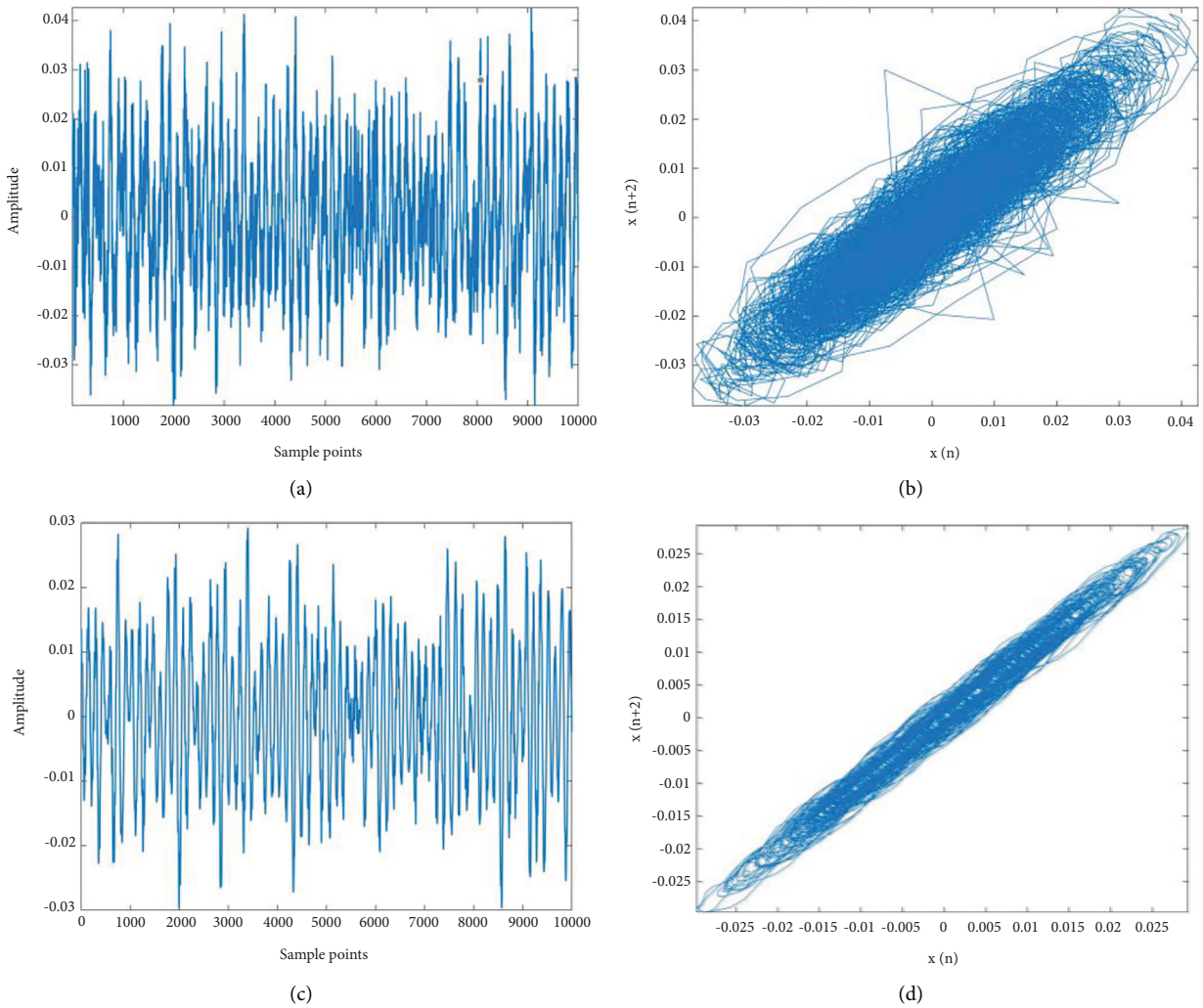

Figure 17: The waveforms and attractor trajectories of original and denoised SN-ii. (a) The waveform of SN-ii. (b) The attractor trajectories of SN-ii. (c) The waveform of denoised SN-ii. (d) The attractor trajectories of denoised SN-ii.

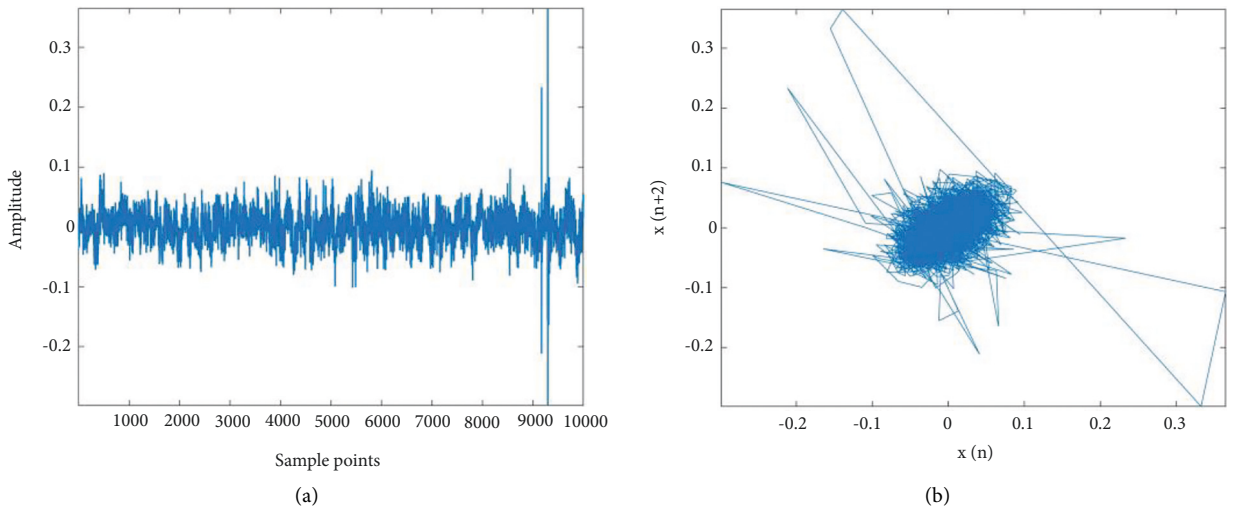

Figure 18: Continued.

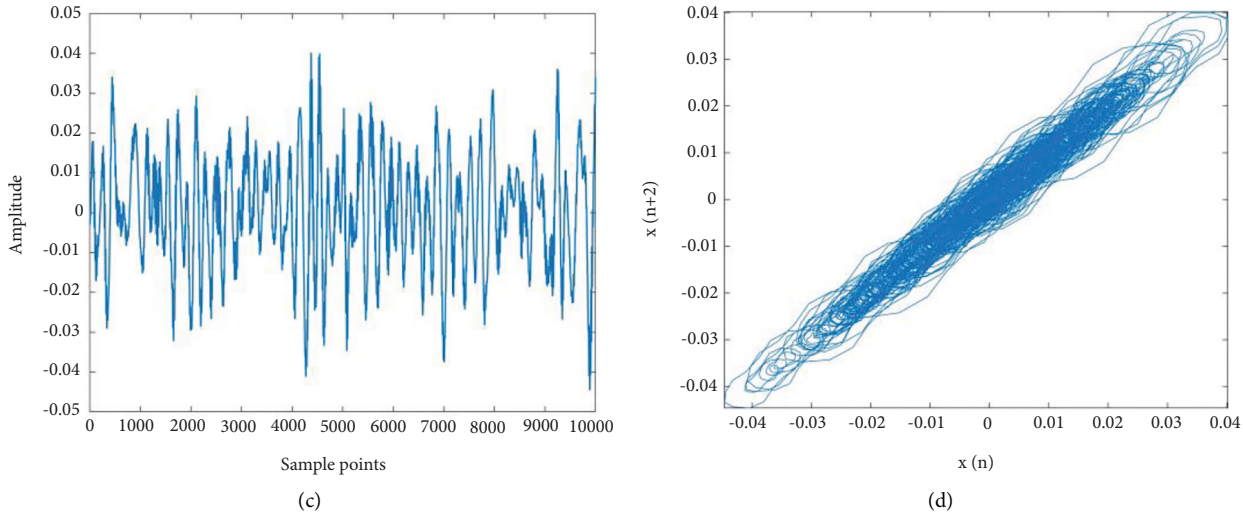

Figure 18: The waveforms and attractor trajectories of original and denoised SN-iii. (a) The waveform of SN-iii. (b) The attractor trajectories of SN-iii. (c) The waveform of denoised SN-iii. (d) The attractor trajectories of denoised SN-iii.

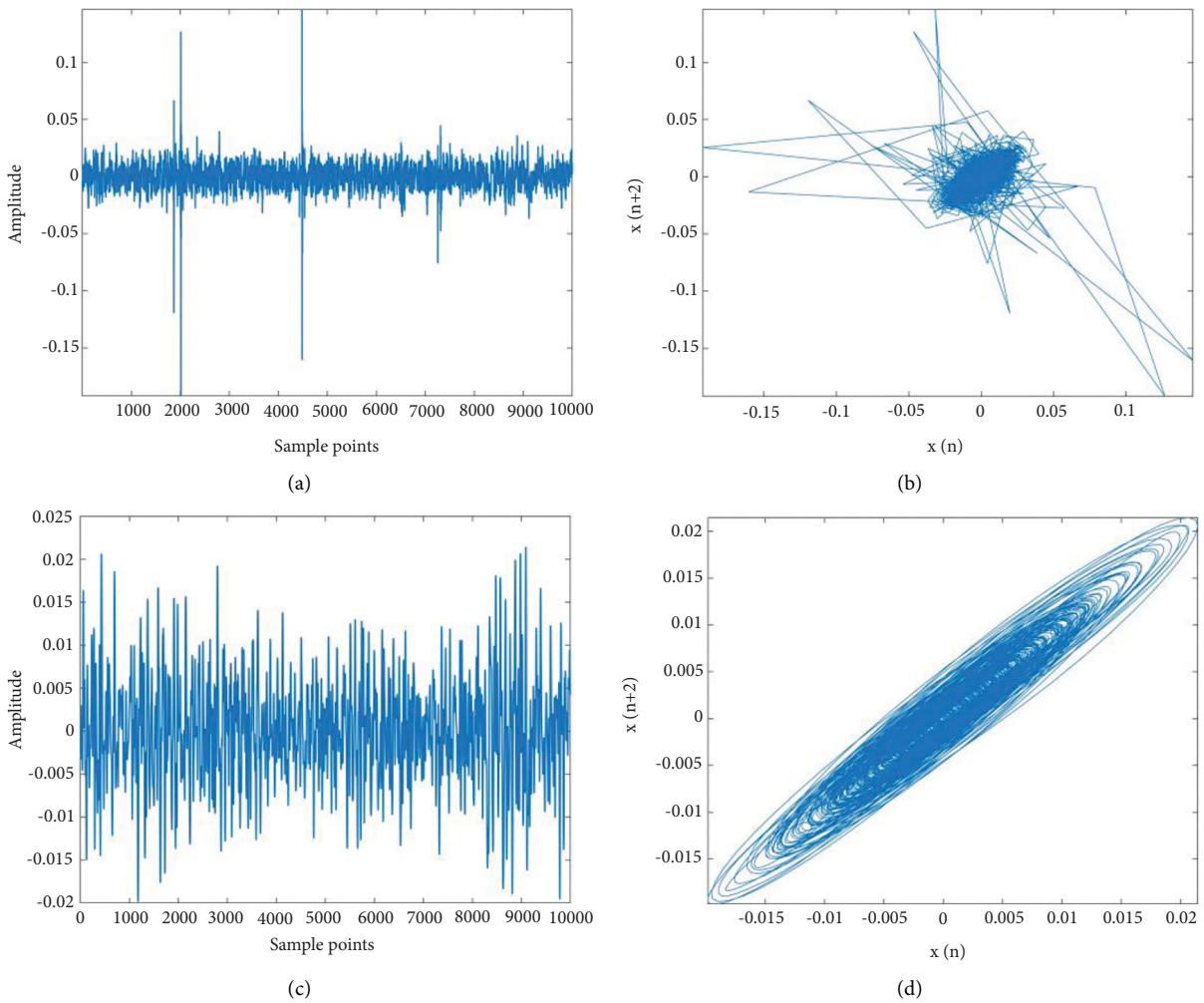

Figure 19: The waveforms and attractor trajectories of original and denoised SN-iv. (a) The waveform of SN-iv. (b) The attractor trajectories of SN-iv. (c) The waveform of denoised SN-iv. (d) The attractor trajectories of denoised SN-iv.

VMD algorithm is ready to start. The decomposition result, that is, the IMFs of SN-iii, is shown in Figure 13.

Eight IMFs have been decomposed precisely. According to the central frequency of each IMF from low to high, they are placed in order and named from IMF1 to IMF8. The amplitude of the first two signals is larger than that of others apparently. A peak of wave repeatedly appears in the range of 9000 to 9500, which tends to be suspected as dramatic noisy impulse.

4.2.2. Classification and Reconstruction. After VMD, calculating the CC of each IMF is essential to classification. At the same time, obtain the dual-threshold with the maximum and the average of CC. The calculated results are given in Figure 14.

The CCs are marked as pentacles in dark blue, and the two horizontal lines are dual-threshold. The blue one is the high threshold and the orange one is the low threshold. Obviously, the IMFs are divided into three parts. The CC of IMF1 is higher than the high threshold over 0.6 actually, and the CC of IMF2 is caught in the middle of two thresholds. The rest of them are under the low threshold with the values hardly reaching 0.2. In accordance with the data above, IMF1 is reckoned as signal component, IMF2 is recognized as signal-noise component, and the rest of IMFs are all noise components. The classification result of SN-iii is shown in Figure 15.

As what is designed previously, IMF1 in blue would be saved, IMF2 in orange is supposed to be denoised with WT, and the rest in gray are unfortunately discarded eventually. Finally, reconstruct them and obtain the final denoising signal.

4.2.3. Results and Analysis. The denoising results of four kinds of SN are displayed in Figures 16–19, which exhibit the waveform and relative attractor trajectories of both original and denoised signals. The trajectories are drawn with the interval of two sample points, so the x-label represents the amplitude of sample point n while the y-label represents the amplitude of $n + 2$.

From the figures above, it can be concluded that after denoising by the proposed method, every waveform is getting cleaner, and furthermore, the attractor trajectories are becoming more regular and smoother. The phenomenon reveals that the proposed method is effective in denoising the SN of all kinds precisely.

5. Conclusions

This paper proposes a brand-new method for denoising SN, which is based on optimized VMD by SO algorithm and dual-threshold criteria of CC. The former is to use SO algorithm and EE to optimize the parameter combination of VMD. The latter is to classify IMFs according to the dual-threshold that is obtained by calculating CC of each IMF. The classified IMFs are processed, respectively, and reconstructed together eventually.

The considerable volume of simulations is performed in this paper so as to verify the distinguished effectiveness of the proposed method. The simulation results not only demonstrate that SO algorithm has more impressive performance than other classical optimizations but also show that the proposed method does better than existing ones in denoising different kinds of test signals with noises to different degrees.

Furthermore, four kinds of SN are introduced and accurately denoised at last. Their attractor trajectories are much cleaner and smoother after denoising, which can powerfully prove that the proposed method is able to denoise the SN of all kinds elaborately.

Data Availability

The data used to support the findings of this study are available from the corresponding author upon request.

Conflicts of Interest

The authors declare that they have no conflicts of interest.

Acknowledgments

This study was supported by the National Natural Science Foundation of China (grant no. U2034209) and the Natural Science Foundation of Shaanxi Province (grant nos. 2022JM-337, 2021JQ-487, and 2020JQ-644).

References

[1] J. D. Tucker and M. R. Azimi-Sadjadi, "Coherence-based underwater target detection from multiple disparate sonar platforms," *IEEE Journal of Oceanic Engineering*, vol. 36, no. 1, pp. 37–51, 2011.

[2] S. Siddagangaiah, Y. Li, X. Guo, and K. Yang, "On the dynamics of ocean ambient noise: two decades later," *Chaos: An Interdisciplinary Journal of Nonlinear Science*, vol. 25, no. 10, Article ID 103117, 2015.

[3] S. Wang and X. Zeng, "Robust underwater noise targets classification using auditory inspired time-frequency analysis," *Applied Acoustics*, vol. 78, no. 4, pp. 68–76, 2014.

[4] S. Siddagangaiah, Y. Li, X. Guo et al., "A complexity-based approach for the detection of weak signals in ocean ambient noise," *Entropy*, vol. 18, no. 3, p. 101, 2016.

[5] N. E. Huang, Z. Shen, S. R. Long et al., "The empirical mode decomposition and the Hilbert spectrum for nonlinear and non-stationary time series analysis," *Proceedings of the Royal Society of London. Series A: Mathematical, Physical and Engineering Sciences*, vol. 454, no. 1971, pp. 903–995, 1998.

[6] Z. Wu and N. E. Huang, "A study of the characteristics of white noise using the empirical mode decomposition method," *Proceedings of the Royal Society of London. Series A: Mathematical, Physical and Engineering Sciences*, vol. 460, no. 2046, pp. 1597–1611, 2004.

[7] A. O. Boudraa and J. C. Cexus, "EMD-Based signal filtering," *IEEE Transactions on Instrumentation and Measurement*, vol. 56, no. 6, pp. 2196–2202, 2007.

[8] O. A. Omitaomu, V. A. Protopopescu, and A. R. Ganguly, "Empirical mode decomposition technique with conditional

mutual information for denoising operational sensor data," *IEEE Sensors Journal*, vol. 11, no. 10, pp. 2565–2575, 2011.

[9] Y. Kopsinis and S. McLaughlin, "Development of EMD-based denoising methods inspired by wavelet thresholding," *IEEE Transactions on Signal Processing*, vol. 57, no. 4, pp. 1351–1362, 2009.

[10] Z. Wu and N. E. Huang, "Ensemble empirical mode decomposition: a noise-assisted data analysis method," *Advances in Adaptive Data Analysis*, vol. 01, no. 01, pp. 1–41, 2009.

[11] Y. Lei, Z. He, and Y. Zi, "Application of the EEMD method to rotor fault diagnosis of rotating machinery," *Mechanical Systems and Signal Processing*, vol. 23, no. 4, pp. 1327–1338, 2009.

[12] J. R. Yeh, J. S. Shieh, and N. E. Huang, "Complementary ensemble empirical mode decomposition: a novel noise enhanced data analysis method," *Advances in Adaptive Data Analysis*, vol. 02, no. 02, pp. 135–156, 2010.

[13] M. E. Torres, M. A. Colominas, G. Schlotthauer, and F. Patrick, "A complete ensemble empirical mode decomposition with adaptive noise," in *Proceedings of the IEEE International Conference on Acoustics, Speech and Signal Processing*, pp. 4144–4147, IEEE, Prague, Czech Republic, May 2011.

[14] H. Lai, "A GPS station noise elimination method combining EEMD and PCA," *Journal of Geomatics*, vol. 47, no. 3, pp. 20–22, 2022.

[15] J. Gu and Y. Peng, "An improved complementary ensemble empirical mode decomposition method and its application in rolling bearing fault diagnosis," *Digital Signal Processing*, vol. 113, Article ID 103050, 2021.

[16] S. Zhao, Y. Zhou, and X. Shu, "Analysis of fiber optic gyroscope dynamic error based on CEEMDAN," *Optical Fiber Technology*, vol. 69, Article ID 102835, 2022.

[17] K. Dragomiretskiy and D. Zosso, "Variational mode decomposition," *IEEE Transactions on Signal Processing*, vol. 62, no. 3, pp. 531–544, 2014.

[18] G. Tang, J. Wang, and H. Luo, "[Fatigue property analysis of prosthesis of hip joint with two different materials]," *Journal of Xi'an Jiaotong University*, vol. 32, no. 1, pp. 73–76, 2015.

[19] Z. Yin, Y. Ren, and W. Feng, "Structural-damage identification based on variational mode decomposition with optimized parameters," *Engineering Construction*, vol. 54, no. 2, pp. 7–13, 2022.

[20] M. Ding, Z. Shi, L. Han, and J. Song, "MEMS gyro signal noise reduction based on optimized VMD-Wavelet threshold," *Journal of Ordnance Equipment Engineering*, vol. 42, no. 8, pp. 191–197, 2021.

[21] H. Li, D. Li, T. Lei, and F. Li, "An optimized VMD algorithm and its application in speech signal denoising," *Journal of Jilin University (Science Edition)*, vol. 59, no. 5, pp. 1219–1227, 2021.

[22] P. Chen and X. Zhao, "Early fault feature extraction of rolling bearing cased on optimized VMD and improved threshold denoising," *Journal of Vibration and Shock*, vol. 40, no. 13, pp. 146–153, 2021.

[23] Y. Li, Y. Li, X. Chen, and J. Yu, "Research on ship-radiated noise denoising using secondary variational mode decomposition and correlation coefficient," *Sensors*, vol. 18, no. 1, p. 48, 2017.

[24] G. Li, Y. Li, and H. Yang, "Noise reduction of ship-radiated noise based on noise-assisted bivariate empirical mode decomposition," *Indian Journal of Geo-Marine Sciences*, vol. 45, no. 4, pp. 469–476, 2016.

[25] Y. Li, Y. Li, X. Chen, and J. Yu, "Denoising and feature extraction algorithms using NPE combined with VMD and their applications in ship-radiated noise," *Symmetry*, vol. 9, no. 11, p. 256, 2017.

[26] Y. X. Li and L. Wang, "A novel noise reduction technique for underwater acoustic signals based on complete ensemble empirical mode decomposition with adaptive noise, minimum mean square variance criterion and least mean square adaptive filter," *Defence Technology*, vol. 16, no. 3, pp. 543–554, 2020.

[27] F. A. Hashim and A. G. Hussien, "Snake Optimizer: a novel meta-heuristic optimization algorithm," *Knowledge-Based Systems*, vol. 242, Article ID 108320, 2022.